Seismic Performance of Masonry Walls Strengthened with Externally Attached Precast Concrete Panels under Cyclic Loading

Xuhong Fan*

Shanxi Polytechnic College, Taiyuan, China

Received 25 May 2026; revised 21 August 2026; accepted 24 August 2026

DOI: https://doi.org/10.46604/ijeti.2026.16476

Abstract

This study aims to develop a low-disruption prefabricated strengthening method to improve the seismic performance of existing masonry walls by externally attaching precast concrete panels. Four masonry wall specimens are tested under quasi-static cyclic loading, including one unstrengthened control wall and three strengthened walls with grouting, shear-key, and combined grouting and shear-key connections. Failure mode, crack development, hysteretic response, energy dissipation, displacement ductility, bearing capacity, and lateral stiffness are evaluated. Results show that the strengthened specimens increase ultimate bearing capacity by 5.92, 5.70, and 5.46 times, respectively, relative to the control specimen, and lateral stiffness by 2.76, 1.94, and 2.30 times, respectively, compared with the control specimen. Grouting improves capacity and stiffness, while shear keys enhance ductility but induce severe local damage. The combined connection provides better deformation compatibility, crack control, and a more balanced seismic performance.

Keywords: masonry wall; precast concrete panel; seismic strengthening; cyclic loading; shear-key connection

1. Introduction

Masonry structures have been widely used in residential, school, office, and public buildings because of their readily available materials, mature construction techniques, and relatively low construction costs. However, many existing masonry buildings were designed and constructed according to earlier seismic design concepts or even without adequate seismic detailing. Owing to the low tensile strength, poor integrity, limited ductility, and insufficient shear resistance of masonry walls, these structures are vulnerable to diagonal cracking, shear failure of wall piers, crushing of wall segments between openings, and rapid degradation of lateral stiffness under earthquake actions [1]. Recent review studies and case-based investigations have further summarized the assessment, repair, and retrofitting strategies for masonry structures and emphasized the need to improve deformation capacity, damage control, and seismic reliability of existing masonry buildings [2–4]. Post-earthquake damage investigations and experimental studies have shown that unstrengthened masonry walls often exhibit brittle failure characteristics and insufficient seismic safety reserve, especially when wall openings, weak mortar joints, or inadequate structural connections are present [1]. Therefore, developing effective strengthening techniques for existing masonry structures remains an important issue in seismic rehabilitation engineering. Traditional strengthening methods for masonry walls mainly include crack grouting, shotcrete or reinforced-concrete overlays, reinforced mortar layers, steel-mesh mortar strengthening, external reinforced-concrete wall jacketing, and post-installed reinforcement [2]. Recent experimental studies have investigated several representative strengthening techniques, including CRM coatings for existing brick masonry walls [5], CRM coatings for stone masonry walls [6], and steel-reinforced plaster systems for retrofitted masonry structures [7]. Similar

* Corresponding author. E-mail address: isadarhzh@126.com

studies have also investigated ferrocement and textile-reinforced mortar systems, polypropylene mesh composites, and other externally applied reinforcement techniques for masonry walls [8–12]. These studies demonstrated that externally applied strengthening layers can improve shear resistance, deformation capacity, and damage control of masonry walls, while also highlighting the importance of interface bonding, reinforcement layout, and local failure mechanisms [5–8, 12, 15]. However, most of these techniques still rely on wet construction processes or continuous surface layers, whereas externally attached precast concrete panels with different connection details have received comparatively limited investigation.

These techniques can improve the bearing capacity, lateral stiffness, and overall integrity of masonry walls through different strengthening mechanisms. For example, shotcrete or reinforced concrete jacketing mainly increases the wall section stiffness and lateral load-bearing capacity; surface-bonded mesh, textile-reinforced mortar, and CRM coating systems are more effective in restraining crack propagation and improving wall integrity; and local reinforcement or anchorage-based methods can enhance shear transfer but may also introduce localized stress concentration. Nevertheless, most conventional methods rely on on-site wet construction and usually require relatively long construction periods, extensive surface treatment, large working space, and strict quality control. For example, recent studies on textile-reinforced concrete strengthening, near-surface-mounted steel wire reinforcement, and twisted-bar or bonded-rebar retrofitting have demonstrated the effectiveness of these methods, but they also involve surface preparation, on-site installation, bonding or mortar layers, and construction quality control requirements [13–15].

In recent years, prefabricated strengthening techniques have attracted increasing attention in the retrofit of existing structures [16]. Compared with cast-in-place concrete or shotcrete strengthening methods, prefabricated components can be manufactured under controlled factory conditions and assembled on site, thereby improving component quality, reducing wet work, and shortening construction time. Recent studies have also explored construction-efficient strengthening strategies, such as self-prestressing reinforced repointing and hybrid GFRP-based configurations, which further reflect the current trend toward lower on-site disturbance, improved construction controllability, and enhanced seismic performance in masonry retrofitting [17, 18]. Strengthening masonry walls with externally attached precast concrete panels is a promising approach. In this method, the added precast panel provides additional lateral stiffness and shear resistance, while the connection between the panel and the original masonry wall enables the two components to resist lateral loads together. Previous studies on masonry-wall strengthening can be broadly classified according to the corresponding strengthening mechanisms. Continuous surface-strengthening systems, including SHCC-based layers, steel-reinforced grout strips, reinforced jacketing, ferrocement overlays, and ECC-based composite overlays, improve lateral resistance, structural integrity, crack control, and energy dissipation by providing an additional load-resisting layer to the original masonry wall [19, 20]. Mechanically anchored or locally connected strengthening systems mainly enhance interfacial shear transfer and anti-slip resistance; however, their performance depends strongly on the anchorage arrangement, connection stiffness, and local stress distribution around discrete connectors [21, 22]. Externally attached precast concrete panels provide additional lateral stiffness and load-bearing capacity while reducing extensive on-site wet construction, but their structural contribution is governed by the load-transfer path and deformation compatibility at the panel-to-wall interface [23, 24].

Zhang et al. [25] previously investigated the seismic behavior of masonry walls strengthened with precast reinforced-concrete panels using different connection details. Their study addressed the same general strengthening concept and evaluated the effects of the connection configuration through failure patterns and global cyclic-response indices, including hysteretic behavior, bearing capacity, stiffness, ductility, and energy dissipation. Therefore, the present study does not claim novelty in either the use of externally attached precast concrete panels or the adoption of grouting, shear-key, and combined grouting–shear-key connections. The results obtained in the present tests are generally consistent with the previous finding that the panel-to-wall connection detail strongly influences the composite cyclic response. More specifically, the grouting connection in the present study provided the highest ultimate bearing capacity and initial lateral stiffness, whereas the shear-key connection was accompanied by severe diagonal cracking, local crushing, and pronounced deformation incompatibility between the precast panel and masonry wall. The combined grouting–shear-key connection did not achieve the highest peak strength but exhibited more favorable crack control and deformation coordination. The present manuscript therefore provides a more focused interpretation of the separately measured panel and masonry-wall deformations and relates the observed deformation mismatch to crack localization, load-transfer characteristics, and the trade-off among strength enhancement, stiffness, deformation compatibility, and local damage. Because only one specimen was tested for each configuration, these comparisons are presented as supplementary and preliminary evidence under the specific specimen and loading conditions adopted in this study.

Previous studies on masonry wall strengthening have demonstrated that strengthening effectiveness is closely related to the retrofit material, connection details, load-transfer mechanism, and deformation compatibility between the added strengthening layer and the original masonry wall [1, 2, 25]. Therefore, the seismic performance of strengthened masonry walls should also be evaluated from multiple aspects, including failure mode, deformation capacity, stiffness degradation, energy dissipation, and load-bearing capacity. To address this issue, this study investigates the seismic performance of masonry walls strengthened with externally attached precast concrete panels under quasi-static cyclic loading. Four masonry wall specimens were designed and fabricated, including one unstrengthened control specimen and three strengthened specimens with different connection methods, namely grouting connection, shear-key connection, and combined grouting and shear-key connection. Because only one specimen was tested for each strengthening configuration, the experimental results are interpreted as preliminary comparative evidence rather than a statistically generalized conclusion. Therefore, the observed differences in bearing capacity, stiffness, ductility, and damage development cannot be attributed exclusively to the connection method, because specimen-to-specimen variability may also have influenced the test results.

To reduce unintended variability, the specimens were designed with the same wall dimensions, brick strength grade, opening configuration, boundary conditions, and vertical loading level, and the measured material properties were reported to support the interpretation of the test results. The failure modes, crack propagation, hysteretic curves, skeleton curves, energy dissipation capacity, displacement ductility, bearing capacity, and lateral stiffness of the specimens were analyzed and compared. The results are expected to provide experimental evidence and design reference for the prefabricated seismic strengthening of existing masonry walls and the optimization of panel-to-wall connection details.

Despite the considerable progress achieved in strengthening masonry walls, several limitations remain in the existing studies. Most strengthening techniques require extensive on-site construction, resulting in long construction periods, significant disturbance to occupants, and difficulties in quality control. In addition, limited research has focused on prefabricated external strengthening systems and the influence of different connection mechanisms on the seismic performance of masonry walls. To provide further comparative evidence on the influence of panel-to-wall connection mechanisms, this study evaluates masonry walls strengthened with externally attached precast concrete panels using grouting, shear-key, and combined grouting–shear-key connections. Rather than proposing a new strengthening concept, the present work focuses on relating the observed failure processes, deformation compatibility, hysteretic response, energy dissipation, bearing capacity, and lateral stiffness to the different interfacial load-transfer mechanisms. The findings provide additional experimental observations for assessing the relative advantages and limitations of the three connection methods. The remainder of this paper is organized as follows. Section 2 presents the specimen design, material properties, and test setup. Section 3 discusses the experimental results, including failure modes, hysteretic behavior, bearing capacity, stiffness degradation, ductility, and energy dissipation. Section 4 summarizes the main conclusions and engineering implications of this study.

2. Experimental Program

2.1 Specimen design and strengthening schemes

To evaluate the effectiveness of externally attached precast concrete panels in improving the seismic performance of existing masonry walls, four masonry wall specimens were designed and fabricated, designated as SW1, SW2, SW3, and SW4. Among them, SW1, SW2, and SW3 were strengthened with externally attached precast concrete panels, whereas SW4 was an unstrengthened masonry wall specimen used as the control specimen. The four specimens had identical masonry wall dimensions, brick strength grade, mortar strength grade, opening configuration, and boundary details, so that the influence of different strengthening schemes could be compared directly. The masonry walls were constructed using MU10 fired clay bricks and M5 mortar. The specimen geometry, masonry details, and material strength grades were designed with reference to the Code for Design of Masonry Structures (GB 50003-2011) and the Code for Seismic Design of Buildings (GB 50011-2010). The reinforced-concrete members and quasi-static cyclic test arrangement were designed with reference to the Code for Design of Concrete Structures (GB 50010-2010) and the Specification for Seismic Test of Buildings (JGJ/T 101-2015), respectively. Appropriate modifications were made to accommodate the laboratory test conditions.

The main material components comprised MU10 fired clay bricks, M5 masonry mortar, post-cast concrete, grouting material, precast-panel concrete, HPB235 reinforcing bars, and Q235 steel sections. Their relevant physical and mechanical properties, including material grades and measured compressive strengths, are reported in Section 2.4 and Table 1. Detailed chemical compositions were not independently measured because these materials were conventional engineering materials, and chemical composition was not an experimental variable in this study. Therefore, no unmeasured chemical-property data are reported. Reinforced concrete loading beams and foundation beams were arranged at the top and bottom of the specimens, respectively, to simulate the boundary conditions and load-transfer path of masonry walls subjected to combined vertical load and horizontal seismic action.

Because specimens SW1–SW3 had identical masonry-wall geometry, opening configuration, boundary members, and precast-panel arrangement, their common configuration is presented once in Fig. 1. The differences among the strengthened specimens are limited to the panel-to-wall connection details, which are presented separately as enlarged sectional views in Fig. 2. Specimen SW4 had the same masonry-wall geometry and boundary members but was not strengthened with a precast concrete panel. The terminology and component labels have been standardized throughout all figures. The construction process of the wall connections and the pouring of the post-cast strips are presented in Figs. 3 and 4, respectively. The common specimen dimensions and reinforcement details are provided in Fig. 5.

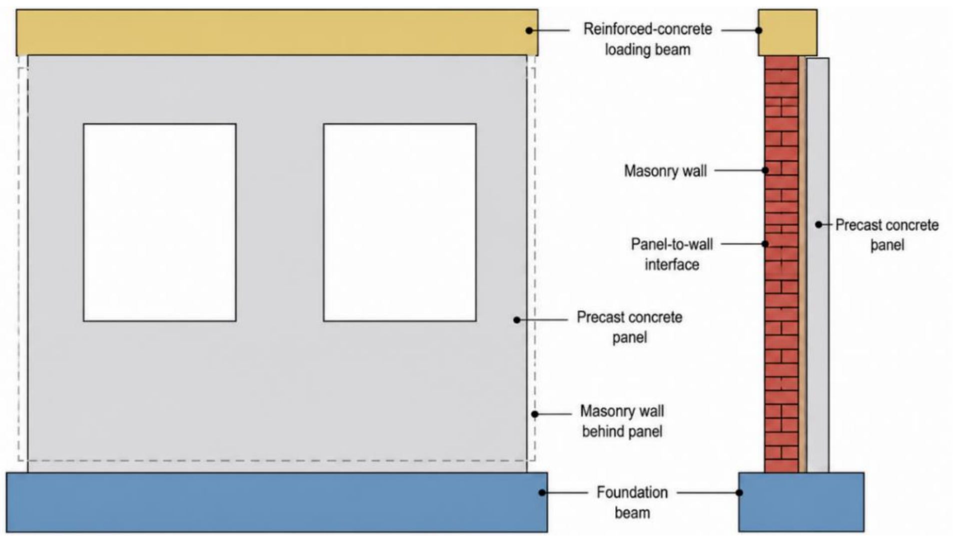

Fig. 1 Common wall geometry and precast-panel arrangement of strengthened specimens SW1–SW3

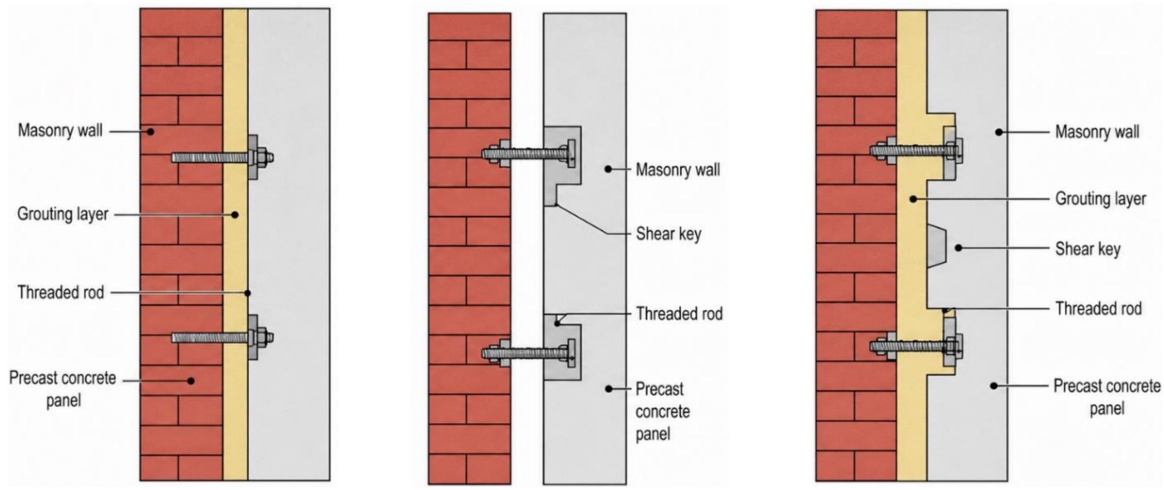

(a) Grouting connection of SW1 (b) Shear-key connection of SW2 (c) Combined grouting and shear-key connection of SW3

Fig. 2 Enlarged sectional views of the panel-to-wall connections

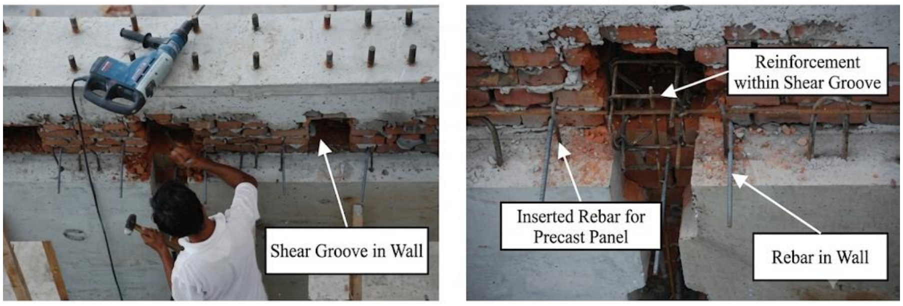

Fig. 3 Construction process of wall connections

Fig. 4 Pouring of post-cast strips in walls

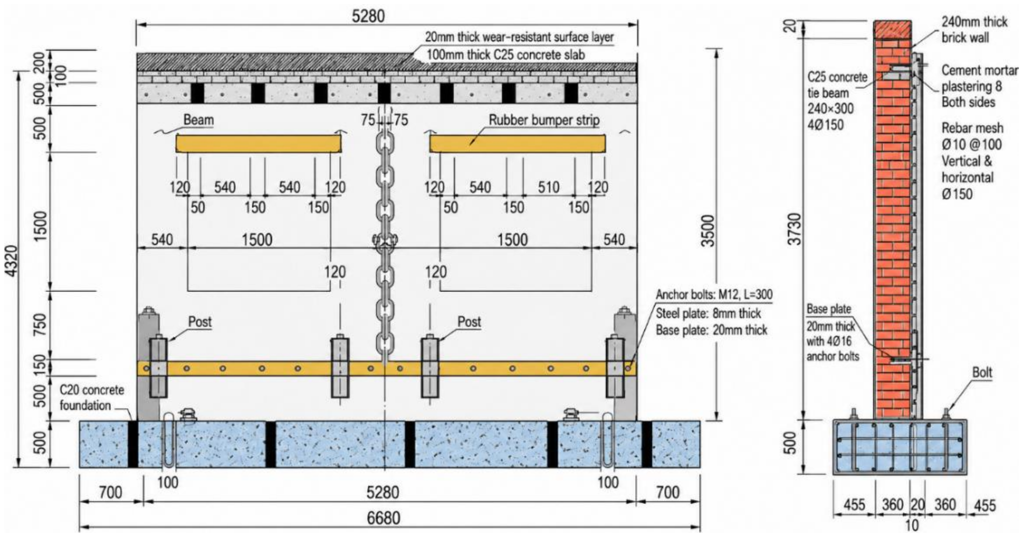

Fig. 5 Dimensions and reinforcement details of the specimen

2.2 Test loading scheme

The specimens were subjected to a constant vertical load and a horizontal quasi-static cyclic load to simulate the stress state of masonry walls under the combined action of gravity load and seismic lateral force. The experimental loading setup is shown in Fig. 6. The loading system consisted of a vertical hydraulic jack serving as the axial loading device, a loading steel beam, a horizontal actuator, four reaction columns, a reinforced-concrete loading beam, a foundation beam, and the reaction floor. The vertical load was applied by the hydraulic jack and transferred to the specimen through the loading steel beam and the reinforced-concrete loading beam. The horizontal cyclic load was applied by the actuator through the loading steel beam.

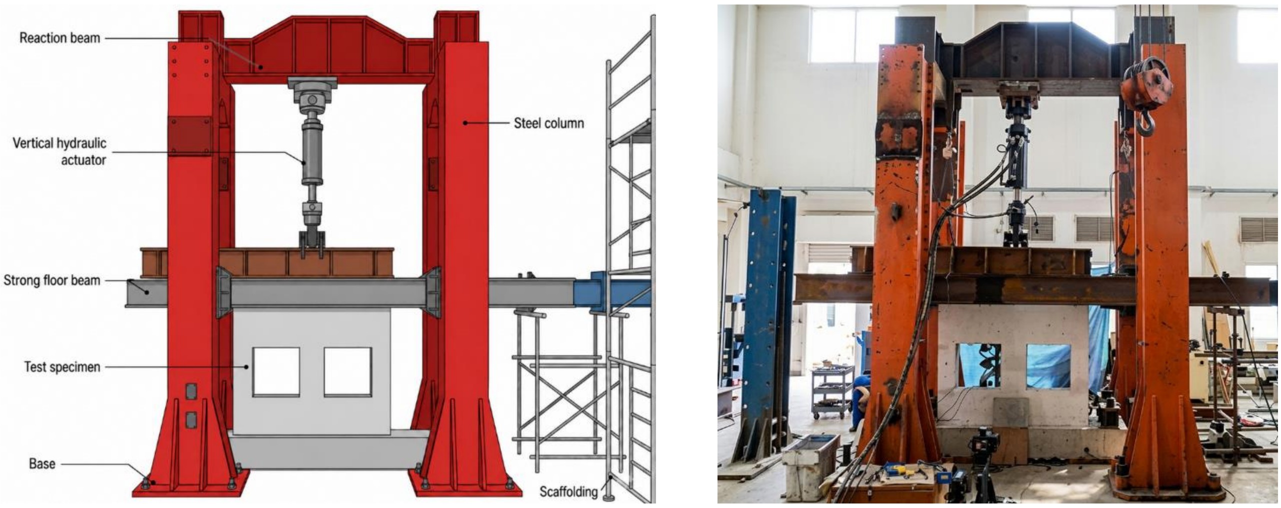

(a) Schematic diagram (b) Photograph

Fig. 6 Experimental loading setup

A reinforced concrete loading beam was cast at the top of each specimen to ensure uniform load transfer along the wall length. The top concrete loading beam was connected to the loading steel beam with bolts, and the loading steel beam served as the primary load-transfer component between the actuator, the vertical loading system, and the specimen. This arrangement was adopted to reduce local stress concentrations at the loading position and to ensure that the horizontal and vertical loads were transmitted to the specimen in a stable, controlled manner.

For vertical loading, a hydraulic jack was used to apply axial compression to the loading steel beam. The vertical load was then transferred from the steel beam to the concrete loading beam and subsequently distributed to the masonry wall specimen. During the entire test, the vertical load was maintained at 294 kN, equivalent to approximately 30 t. This load level was selected to represent the sustained gravity-induced axial compression acting on the masonry walls and to maintain the specimens under a stable compression state during horizontal cyclic loading. Based on the net cross-sectional area of the masonry wall, the applied vertical load corresponded to a moderate axial compression level and remained below the compressive capacity of the specimen, thereby avoiding premature compression failure before lateral loading. The same vertical load was applied to all specimens to ensure consistent axial loading conditions and facilitate comparison among the different strengthening schemes. The vertical loading system was monitored throughout the test to ensure that the axial force remained approximately constant during horizontal cyclic loading.

For horizontal loading, an electro-hydraulic servo actuator was used to apply a lateral cyclic force to the specimen. One end of the actuator was connected to the laboratory reaction wall, while the other end was connected to the loading steel beam at the top of the specimen. The horizontal load was therefore applied to the specimen through the loading steel beam and the top concrete loading beam. The loading protocol was performed in a quasi-static cyclic manner. This loading procedure was designed with reference to the Specification for Seismic Test of Buildings (JGJ/T 101-2015), and similar force-controlled-to-displacement-controlled quasi-static cyclic loading protocols have been adopted in previous experimental studies on masonry walls and strengthened masonry wall specimens [19–22, 25]. In the initial elastic stage, force-controlled loading was adopted to accurately capture the initial stiffness and early cracking behavior of the specimens. After the specimen reached the yielded stage and its lateral stiffness had degraded significantly, the loading mode was changed to displacement control to investigate the post-yield deformation capacity, hysteretic behavior, stiffness degradation, and failure process.

The direction in which the actuator pushed the specimen was defined as the positive loading direction, while the opposite direction was defined as the negative loading direction. The test was terminated when the lateral bearing capacity decreased to a proportion of the peak load or when severe cracking, local crushing, or potential instability was observed in the specimen.

2.3 Measurement scheme

The measurement arrangement was designed to capture the global lateral response, local shear deformation, deformation compatibility between the masonry wall and the externally attached precast concrete panel, and strain development in key structural components. The overall measurement scheme is shown in Fig. 7. A total of nine wire-draw displacement transducers and nineteen strain gauges were installed during the test. The wire-draw displacement transducers were used to measure horizontal displacement, relative slip, and local deformation of the specimens. The strain gauges were electrical resistance foil strain gauges and were attached to the reinforcement, threaded rods, and other key components to monitor strain development during cyclic loading.

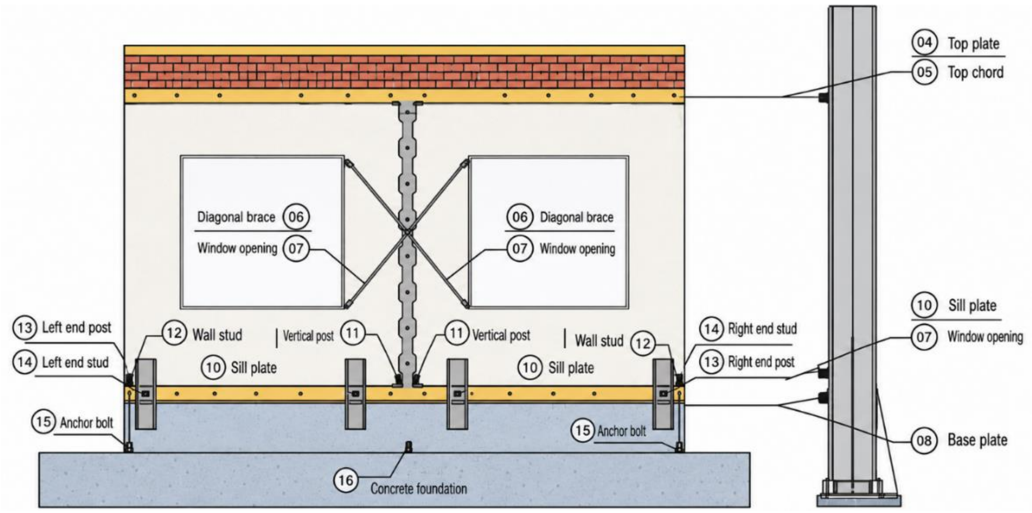

Fig. 7 Measurement arrangement of the specimen

The wire-draw displacement transducers were used to measure both global and local deformation responses of the specimens. Transducers D5–D9 were primarily configured to measure the lateral displacement of the wall system. Since the strengthened specimens consisted of the original masonry wall and the externally attached precast concrete panel, the lateral displacements of both components were measured to evaluate their collaborative deformation during cyclic loading. Transducers D1–D4 were arranged diagonally around the window opening to measure the shear deformation of the wall pier between openings. For the strengthened specimens, the diagonal deformation of the masonry wall and that of the externally attached precast concrete panel were measured separately, allowing evaluation of the relative deformation and compatibility between the two components.

Strain gauges were installed to monitor the strain response of the steel components and the precast concrete panel. Strain gauges S1–S12 were arranged on the steel sections or connection-related steel components to record the tensile and shear strain development during loading. Strain gauges S13–S19 were attached to the precast concrete panel to identify potential stress-concentration regions and capture the strain evolution associated with cracking and damage development. These measurements provided essential data for evaluating the load-transfer mechanism and the interaction between the precast concrete panel and the masonry wall.

The lateral displacement was measured using SW-40 relative displacement transducers, while the shear deformation was measured using DP-500E and DP-1000E displacement transducers manufactured by Tokyo Measuring Instruments Laboratory. Electrical resistance foil strain gauges were installed at measuring points S1–S19 to monitor the strain responses of the relevant structural components. All load, displacement, and strain signals were recorded using a TDS-530 data acquisition system. Before testing, all displacement transducers and strain-measurement channels were calibrated and zeroed after installation.

2.4 Material test results

To determine the actual mechanical properties of the materials used in the specimens, cube compression tests were conducted on the mortar, post-cast concrete, grouting material, and precast wall panel concrete. The measured compressive strengths are summarized in Table 1. The values listed in the table are the average strengths obtained from the corresponding material test specimens. It should be noted that noticeable differences existed among the measured compressive strengths of some materials. These differences may be attributed to batch-to-batch variation, differences in mixing and casting procedures, local compaction quality, curing conditions, and the inherent variability of cement-based materials and masonry mortar. In particular, the post-cast concrete and mortar were prepared and cast during specimen fabrication, and their measured strengths may therefore reflect normal construction-related variability. Such material-strength variation may have influenced the local stiffness, cracking behavior, and load-transfer capacity of the specimens and is therefore considered when interpreting the experimental results. Accordingly, the differences in seismic performance are not attributed solely to the connection methods.

Table 1 Material test results (unit: MPa)

Specimen	Post-cast concrete	Mortar	Grouting material	Precast wall panel concrete
SW1	18.54	2.00	12.43	32.69
SW2	27.76	1.95	—	32.69
SW3	27.36	2.44	12.94	32.69
SW4	—	2.16	—	N/A

Note: N/A indicates that no precast wall panel was used in the unstrengthened control specimen SW4.

For the cube compression tests, the specimen dimensions were selected according to the material type, aggregate characteristics, and molding and testing requirements. Cubes with a side length of 150 mm were used for the post-cast concrete and masonry mortar, cubes with a side length of 71 mm were used for the grouting material, and cubes with a side length of 100 mm were used for the precast wall panel concrete. The different cube dimensions were adopted to accommodate the material characteristics and laboratory molding conditions and to obtain representative compressive-strength results. The masonry walls were constructed using fired common bricks with a strength grade of MU10 and M5 masonry mortar. HPB235 steel was used for the reinforcement, while Q235 structural steel was used for the I-shaped components of the loading steel beam and auxiliary loading frame rather than for the masonry wall or the strengthening system. The I-shaped cross-section was selected because it provided sufficient flexural stiffness and load-transfer capacity while limiting deformation of the loading apparatus under the forces applied by the horizontal actuator and vertical hydraulic jack. These members served only as loading and boundary-restraint components and did not contribute to the seismic resistance of the test specimen. The materials used varied among the different strengthening schemes. The grouting material was mainly used in the specimens with a grouting connection or a combined grouting and shear-key connection. Therefore, no grouting material strength is reported for the unstrengthened control specimen. Similarly, the post-cast concrete and precast wall panel concrete strengths are reported only for the specimens that used the corresponding materials.

It should be noted that the post-cast concrete strength varied among the strengthened specimens, with SW1 showing a lower measured strength (18.54 MPa) than SW2 (27.76 MPa) and SW3 (27.36 MPa). Although this variation may have introduced a certain influence on the local stiffness and strength of the strengthened specimens, the overall experimental results suggest that the connection mechanism played a more dominant role in determining the seismic performance. If the post-cast concrete strength had been the governing factor, SW2 and SW3 would be expected to contribute to higher bearing capacities and lateral stiffness than SW1. However, the test results showed the opposite trend. This observation is consistent with the influence of the continuous grouting connection; however, because only one specimen was tested for each configuration, the influences of the connection method, material variability, construction quality, and interface bonding cannot be separated quantitatively. Therefore, the observed differences are interpreted as preliminary experimental trends rather than conclusive effects caused solely by the strengthening schemes.

2.5 Loading protocol

A quasi-static reversed cyclic loading protocol was adopted to evaluate the seismic behavior of the masonry wall specimens. The loading procedure was designed with reference to the Specification for Seismic Test of Buildings (JGJ/T 101-2015). A similar force-controlled-to-displacement-controlled quasi-static cyclic loading protocol has been adopted in previous experimental studies on masonry walls strengthened with precast reinforced-concrete panels [25]. In the initial approximately elastic stage, force-controlled loading was used to determine the initial stiffness and cracking response. After yielding and significant lateral stiffness degradation, the loading mode was changed to displacement control to investigate the post-yield deformation capacity, hysteretic response, stiffness degradation, and failure process.

Force control was applied only during the early loading stage, and the transition to displacement control was determined according to the initial lateral resistance, observed cracking behavior, and test safety of each specimen rather than a uniform prescribed force level. For SW1, the continuous grouting connection provided relatively stable load transfer and higher initial lateral resistance; therefore, force-controlled loading was continued up to 320 kN, as shown in Fig. 8.

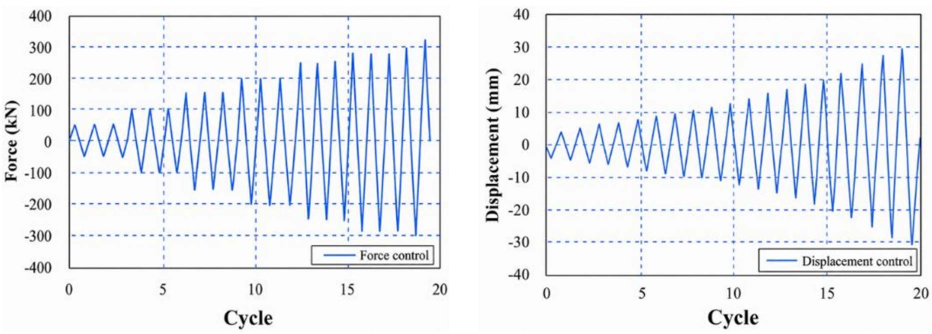

(a) Force control (b) Displacement control

Fig. 8 Loading history of specimen SW1

For SW2 and SW3, which incorporated shear-key connections, the force-controlled stage was limited to 200 kN to reduce the risk of premature localized damage before displacement-controlled cycling, as presented in Figs. 9 and 10, respectively. The unstrengthened control specimen SW4 was directly subjected to displacement-controlled loading because of its relatively low lateral resistance and potentially brittle response, thereby allowing more stable control of its deformation response, as shown in Fig. 11.

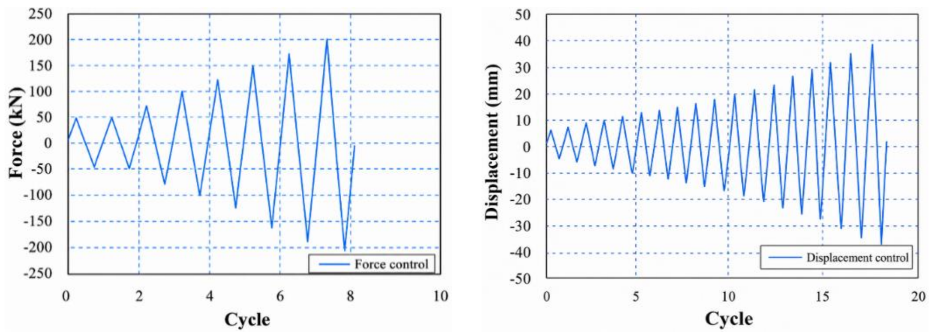

(a) Force control (b) Displacement control

Fig 9 Loading history of specimen SW2

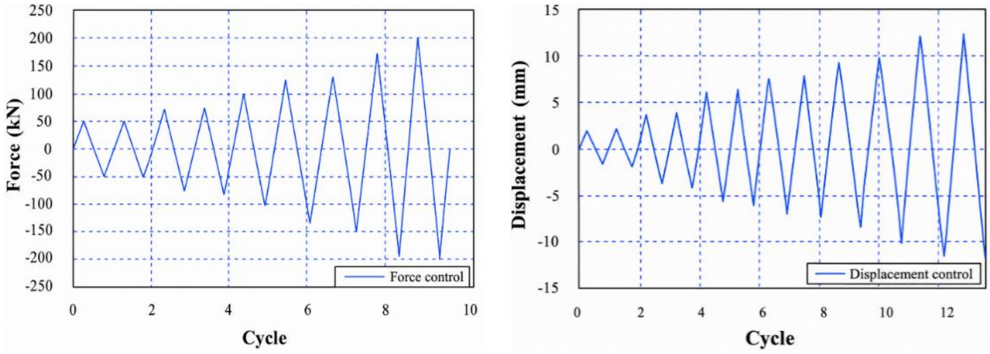

(a) Force control (b) Displacement control

Fig. 10 Loading history of specimen SW3

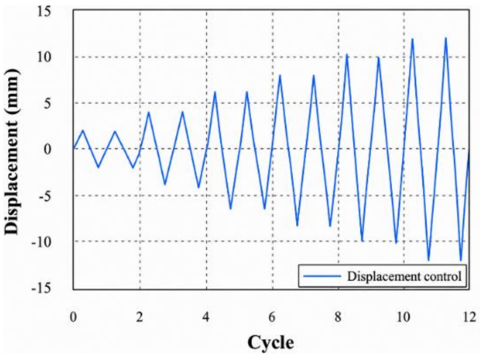

Fig. 11 Loading history of specimen SW4

Consequently, the four specimens did not experience identical loading histories before displacement-controlled cycling, which may have influenced their accumulated damage states. This limitation was considered by interpreting the load–displacement responses together with the observed crack propagation, interface damage, and failure modes rather than attributing the measured differences solely to the connection method.

Under displacement-controlled loading, the maximum applied displacement amplitude reached 30 mm for specimens SW1 and SW3, and 40 mm for specimen SW2. In general, the test was terminated when the lateral bearing capacity of a specimen decreased to approximately 80% of its peak load, or when severe cracking, local crushing, or potential instability was observed.

Specimen SW2 was an exception. During the test, severe crack propagation occurred in the wall pier between openings, accompanied by significant local damage. Considering the potential risk of local collapse, the loading of specimen SW2 was terminated before the bearing capacity dropped to the specified threshold. Therefore, the maximum displacement of SW2 should not be interpreted as a stable ultimate deformation capacity, but rather as the displacement level reached before the test was prematurely terminated due to severe local damage.

3. Experimental Phenomena Analysis

Figs. 12–14 show the crack patterns of the strengthened specimens SW1–SW3 at representative displacement amplitudes. In each figure, subfigure (a) presents the crack distribution at the early or intermediate loading stage, whereas subfigure (b) shows the crack development at the later loading stage. Table 2 summarizes the diagonal displacement measured by the wire-draw displacement transducers arranged in the wall pier between openings under typical displacement amplitudes. These measurements were used to evaluate the shear deformation of the masonry wall and the externally attached precast concrete panel, and to assess their deformation compatibility during cyclic loading. The results are further analyzed to assess the effects of different connection methods on damage development and deformation compatibility.

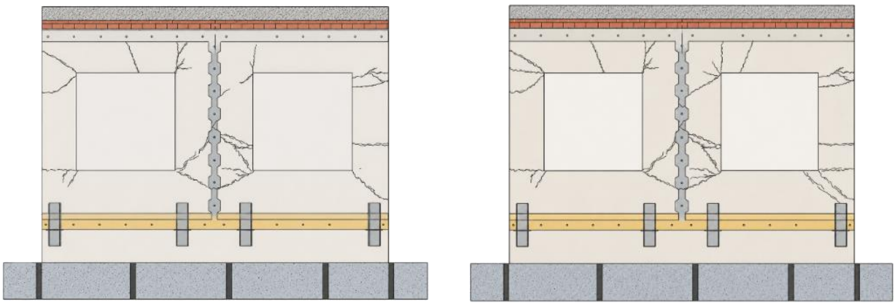

(a) Crack pattern at 9 mm displacement (b) Crack pattern at 21 mm displacement

Fig. 12 Crack pattern of specimen SW1

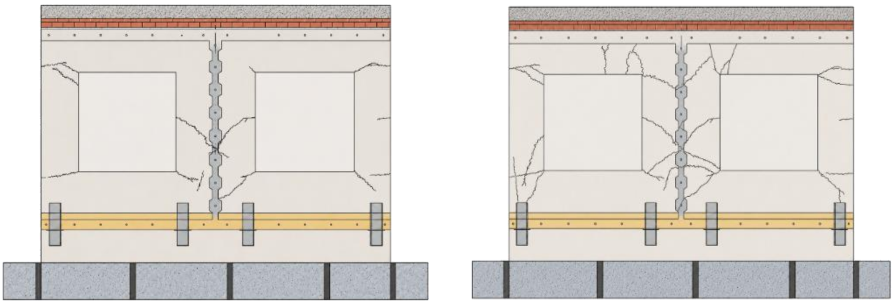

(a) Crack pattern at 8 mm displacement (b) Crack pattern at 22 mm displacement

Fig. 13 Crack pattern of specimen SW2

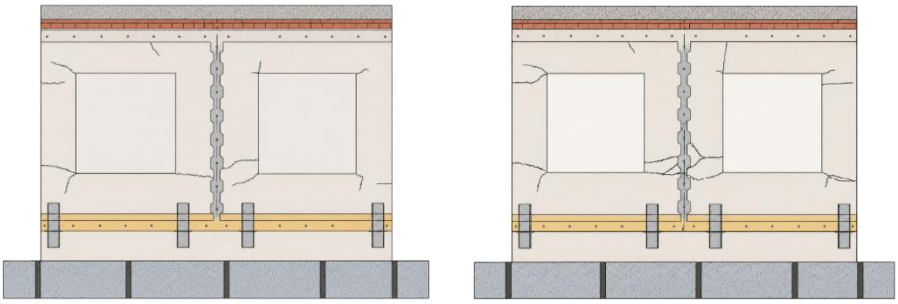

(a) Crack pattern at 9 mm displacement (b) Crack pattern at 23 mm displacement

Fig. 14 Crack pattern of specimen SW3

As shown in Figs. 12–14, the cracks in the strengthened specimens mainly consisted of diagonal cracks at the corners of the window openings, horizontal cracks at the bottom of the wall pier between openings, and diagonal shear cracks within the wall pier. These crack patterns are typical of masonry walls subjected to cyclic lateral loading. However, the crack development varied significantly with the connection method between the externally attached precast concrete panel and the original masonry wall.

For specimen SW1, which was strengthened using a grouting connection, the initial cracks mainly appeared at the corners of the window openings and the lower part of the wall pier. As the displacement amplitude increased, diagonal cracks gradually developed within the wall pier, and horizontal cracks appeared near the bottom region. The crack distribution of SW1 was relatively controlled, indicating that the continuous grouting layer provided an effective interfacial restraint between the precast concrete panel and the masonry wall. Nevertheless, at larger displacement amplitudes, the repeated opening and closing of cracks led to progressive damage accumulation, and a certain degree of deformation incompatibility between the panel and the masonry wall was observed.

Specimen SW2, strengthened by a shear-key connection, exhibited the most severe cracking among the three strengthened specimens. When the displacement amplitude reached approximately 20 mm, the wall pier between openings showed extensive diagonal cracking, with crack lengths greater than those in SW1 and SW3. The crossed diagonal cracks in the wall pier became particularly evident, and local crushing occurred in the lower part of the masonry wall. These observations suggest that the shear-key connection could transfer horizontal shear force through localized mechanical interlocking, but the load transfer was concentrated around the shear-key regions. As a result, local stress concentration developed in the masonry wall, leading to rapid crack propagation and severe local damage.

For specimen SW3 strengthened by the combined grouting and shear-key connection, fewer and less extensive cracks were observed than in SW1 and SW2 at similar displacement amplitudes. The cracks were mainly distributed around the window corners and the lower part of the wall pier, while the diagonal cracks within the wall pier developed more slowly. This phenomenon indicates that the combined connection effectively integrated the continuous interfacial bonding provided by grouting and the localized mechanical anchorage provided by shear keys. As a result, the externally attached precast concrete panel and the masonry wall exhibited better collaborative behavior, and the damage development was more effectively restrained.

The diagonal displacement measurements in Table 2 further illustrate the influence of connection methods on deformation compatibility. For specimen SW2, when the displacement amplitude reached +25 mm, the diagonal displacement of the precast concrete panel was 5.5 mm, whereas that of the masonry wall reached 49.8 mm. Under the −25 mm displacement amplitude, the corresponding diagonal displacements of the precast concrete panel and the masonry wall were 23.5 mm and 44.7 mm, respectively. The large difference between the panel and the masonry wall indicates poor deformation compatibility and severe shear deformation of the masonry wall. In contrast, specimen SW3 showed much smaller differences between the diagonal displacements of the precast concrete panel and the masonry wall. At a displacement amplitude of 27 mm, the diagonal displacements of the panel and masonry wall were 8.1 mm and 5.0 mm in the positive direction, and 8.95 mm and 7.7 mm in the negative direction, respectively. This indicates that the combined grouting and shear-key connection provided better deformation coordination between the two components.

Table 2 Diagonal displacements of the wall pier between openings under typical displacement amplitudes (unit: mm)

Specimen	Displacement amplitude	Positive direction		Negative direction	
		Concrete panel	Brick wall	Concrete panel	Brick wall
SW1	21	26	16.9	11.5	0.3
SW2	25	5.5	49.8	23.5	44.7
SW3	27	8.1	5	8.95	7.7

Although specimen SW2 could still maintain a certain level of horizontal bearing capacity at large displacement amplitudes, severe cracking and local crushing had already occurred in the wall pier between openings. This damage may compromise the wall's vertical load-bearing capacity and amplify the adverse influence of the P–δ effect under large lateral deformation. Therefore, the shear-key connection alone improved mechanical interlocking but was insufficient to effectively control crack development and local damage. In comparison, the grouting connection provided better crack restraint, while the combined grouting and shear-key connection showed the best overall performance in terms of crack control, deformation compatibility, and collaborative action between the precast concrete panel and the masonry wall.

Overall, the experimental phenomena indicate that all three strengthening schemes changed the damage development of the masonry walls to different extents. The grouting connection was effective in restraining crack propagation through continuous interfacial bonding. The shear-key connection enhanced local mechanical interaction but caused pronounced stress concentration and severe cracking in the masonry wall. The combined grouting and shear-key connection provided more balanced load transfer and better deformation compatibility, resulting in the most favorable crack-control performance among the three strengthening schemes.

4. Seismic Performance Evaluation

4.1 Hysteretic curves, skeleton curves, and energy dissipation curves

The hysteretic curves of the four specimens are shown in Fig. 15. The skeleton curves obtained from the peak load points of the first cycle at each displacement level are compared in Fig. 16. The cumulative energy dissipation curves are presented in Fig. 17. These curves were used to evaluate the lateral load-bearing capacity, stiffness degradation, deformation capacity, and energy dissipation behavior of the masonry wall specimens with different strengthening schemes.

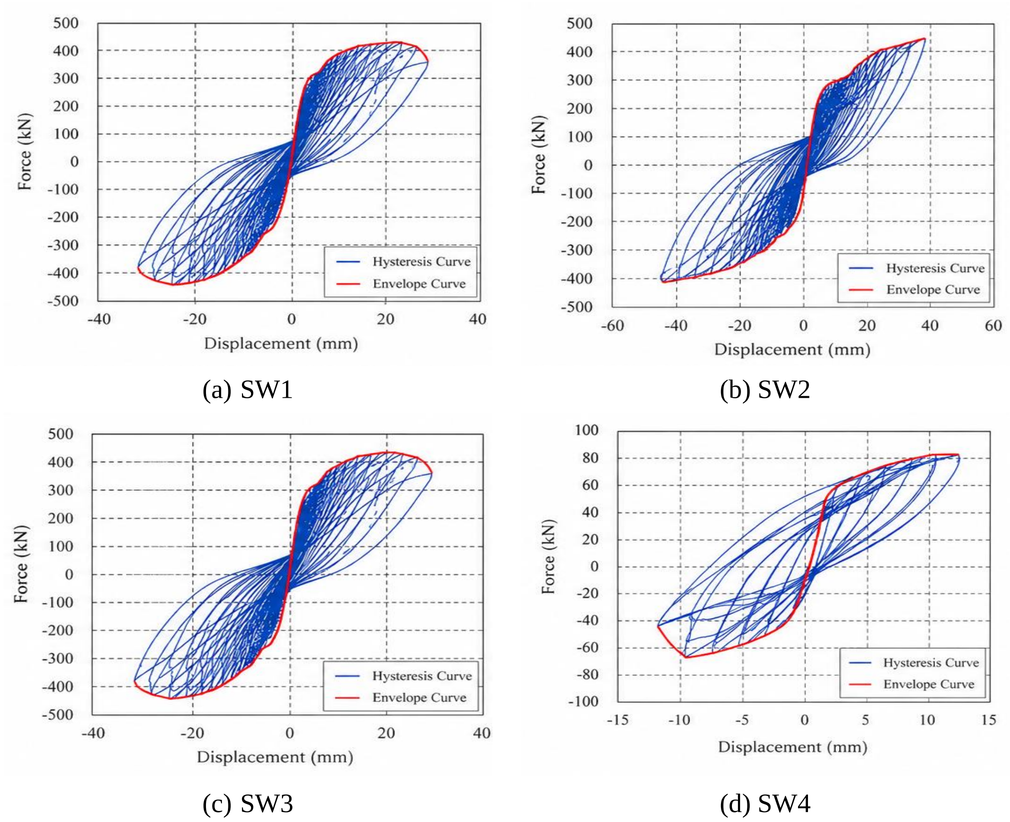

(a) SW1 (b) SW2

(c) SW3 (d) SW4

Fig. 15 Hysteretic curves of the specimens

As shown in Fig. 15, the unstrengthened specimen SW4 exhibited relatively narrow hysteretic loops, limited load-bearing capacity, and rapid stiffness degradation, indicating inferior seismic performance of the original masonry wall. In contrast, the hysteretic loops of the strengthened specimens SW1, SW2, and SW3 were significantly larger, indicating that the externally attached precast concrete panels enhanced the lateral resistance and energy dissipation capacity of the masonry wall system.

The hysteretic curves of specimens SW1 and SW3 were relatively full and showed similar overall shapes. At the initial loading stage, the curves exhibited a spindle-shaped pattern, suggesting that the specimens maintained good integrity and relatively stable load-transfer capacity before severe cracking occurred. With increasing displacement amplitude, diagonal cracks gradually developed and repeatedly opened and closed during cyclic loading. As a result, the hysteretic curves gradually showed a pinching effect and evolved into an inverse S-shaped pattern. This behavior is typical of masonry-dominated systems subjected to cyclic lateral loading and is characterized by crack opening and closing, local sliding, stiffness degradation, and damage accumulation.

Among the three strengthened specimens, SW2 exhibited the most pronounced stiffness degradation. Although the lateral bearing capacity of SW2 continued to increase during part of the loading process, severe cracking and local crushing had already occurred in the wall pier between openings, as discussed in Section 3. The rapid reduction in the slope of the hysteretic curves is consistent with the more localized damage and weaker deformation compatibility between the precast concrete panel and the masonry wall. In comparison, SW3 showed more stable hysteretic behavior, which may be attributed to the combined effects of continuous interfacial bonding from grouting and localized mechanical anchorage from shear keys.

The skeleton curves in Fig. 16 further demonstrate the strengthening effect of the externally attached precast concrete panels. Compared with SW4, the peak lateral loads of SW1, SW2, and SW3 were substantially higher. The peak points and descending branches were used to compare the lateral resistance and post-peak response of the specimens. Specimen SW1 exhibited the highest peak load, indicating that the grouting connection enhanced the overall lateral bearing capacity through continuous interfacial bonding. Specimen SW2 exhibited relatively large deformation capacity, but its damage developed more severely. Specimen SW3 had a slightly lower peak load than SW1, but its damage process was more stable, and its panel-to-wall collaborative behavior was better. Therefore, the performance of the strengthened specimens should be evaluated not only by peak load, but also by stiffness degradation, crack control, deformation compatibility, and damage development.

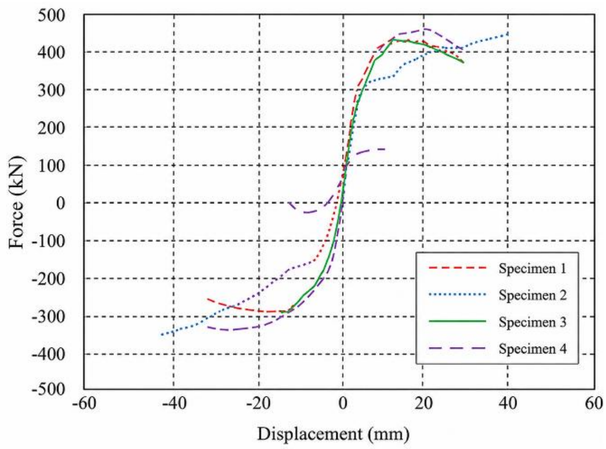

Fig. 16 Comparison of skeleton curves

The cumulative energy dissipation curves in Fig. 17 were obtained by summing the energy dissipated by the specimens at the end of each loading cycle. The horizontal axis represents the displacement amplitude of a given loading cycle, while the vertical axis represents the accumulated energy dissipation. Because different specimens underwent different numbers of cycles during the force-controlled loading stage, the energy values at a displacement amplitude of 2 mm were used as the reference point for the strengthened specimens to facilitate comparison.

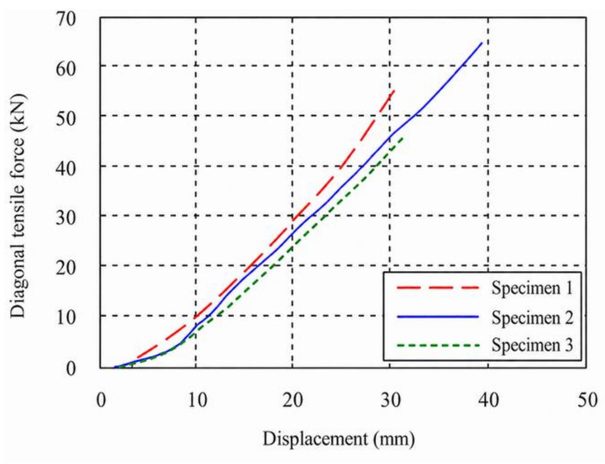

Fig.17 Cumulative energy dissipation curves

As shown in Fig. 17, the energy dissipation capacity of the strengthened specimens was much higher than that of the unstrengthened specimen SW4. The strengthened specimens exhibit larger accumulated energy values than SW4 at comparable displacement amplitudes. This indicates that the externally attached precast concrete panels improved the masonry wall’s seismic energy dissipation capacity. Although specimen SW2 showed relatively high cumulative energy dissipation at large displacement amplitudes, this was accompanied by severe crack propagation, local crushing, and poor deformation compatibility between the masonry wall and the precast concrete panel. Therefore, its energy dissipation was achieved at the cost of considerable local damage. In contrast, specimen SW3 exhibited better crack control and more coordinated deformation between the wall and the panel. From the combined perspectives of energy dissipation, damage control, and collaborative working performance, the grouted shear-key connection adopted in SW3 provided the most balanced seismic performance among the three strengthening schemes.

4.2 Displacement ductility

The displacement ductility coefficient, β_ω, was calculated as：

$$\beta_\omega = \frac{\omega_u}{\omega_y} \tag{1}$$

where ω_y is the yield displacement and ω_u is the displacement corresponding to the maximum lateral bearing capacity. Therefore, in the present study, ω_u was operationally defined as the peak-load displacement rather than the displacement corresponding to a specified post-peak strength-degradation level. Accordingly, β_ω is interpreted as a dimensionless peak-load-based displacement ductility index for comparing the deformation characteristics of the specimens.

The yield point $Y(\omega_y, F_y)$ was determined from the skeleton curve using the geometric drawing method illustrated in Fig. 18. First, line *OA* was drawn tangent to the initial approximately linear segment of the skeleton curve and extended to intersect the horizontal line passing through the peak-load point $U(\omega_u, F_u)$ at point *A*. A vertical line from *A* was then drawn to intersect the skeleton curve at point *B*. Line *OB* was extended to intersect the horizontal line through *U* at point *C*, and a vertical line through *C* intersected the skeleton curve at point *Y*. The corresponding ω_y and F_y were then used to calculate β_ω.

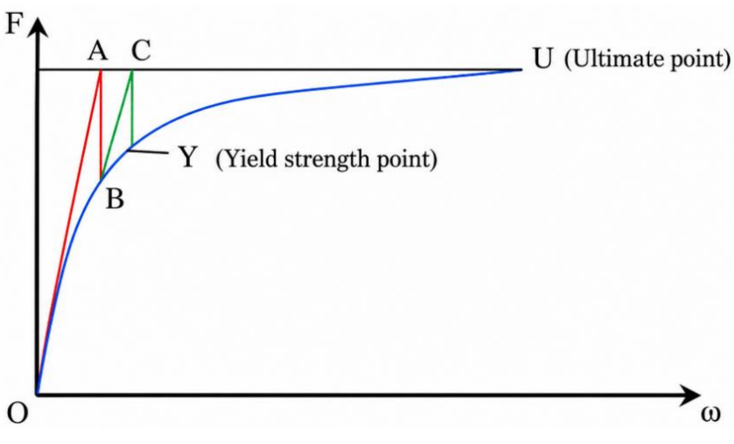

Fig. 18 Geometric drawing method for determining the yield point

For SW2, the test was terminated before a complete post-peak response was obtained because of severe local cracking and the risk of collapse. Therefore, its reported coefficient represents a nominal peak-load-based ductility index derived from the available experimental response and should not be regarded as a fully developed ultimate deformation capacity.

Using the above procedure, the peak lateral force F_u, peak-load displacement ω_u, yield force F_y, yield displacement ω_y, and corresponding peak-load-based displacement ductility index β_ω were determined for all four specimens, as summarized in Table 3. Specimen SW4 was included as the unstrengthened baseline for evaluating the influence of the different strengthening schemes on deformation capacity.

Table 3 Peak-load-based displacement ductility indices of all specimens

Specimen	SW1	SW2	SW3	SW4
F_u(kN)	450	433	415	76
ω_u(mm)	20.5	37.9	12.2	4.0
F_y(kN)	343	293	350	57.1
ω_y(mm)	6.7	9.2	7.7	2.0
Displacement ductility coefficient, β_ω	3.05	4.12	1.58	2.00

Note: For SW2, ω_u corresponds to the maximum displacement reached before premature test termination due to severe local damage. For SW4, the reported value was calculated from the available skeleton curve and is used only as an unstrengthened baseline because the specimen exhibited rapid post-yield strength degradation. Therefore, the values for SW2 and SW4 should be interpreted as nominal peak-load-based ductility indices rather than fully developed ultimate deformation capacities.

As shown in Table 3, the nominal peak-load-based displacement ductility index of the unstrengthened specimen SW4 was 2.00. Compared with SW4, the indices of SW1 and SW2 were 52.5% and 106.0% higher, respectively, whereas that of SW3 was 21.0% lower. These results indicate that the grouting connection used in SW1 increased the deformation attained after yielding, while the relatively large nominal index of SW2 was accompanied by severe cracking, local crushing, and premature test termination. Although SW3 exhibited a lower ductility index than SW4, it provided substantially higher bearing capacity, better crack control, and more coordinated panel-to-wall deformation. Therefore, the effectiveness of the strengthening schemes should not be assessed solely from the displacement ductility index but should be evaluated together with bearing capacity, damage development, stiffness degradation, and deformation compatibility.

Specimen SW2 strengthened with the shear-key connection exhibited the largest peak-load-based displacement ductility index of 4.12. However, severe diagonal cracking and local crushing in the wall pier between openings led to premature termination of the test before the lateral resistance decreased to 80% of the peak load. Therefore, the reported displacement of 37.9 mm represents the maximum displacement recorded before test termination rather than a conventionally defined ultimate displacement obtained from a complete post-peak response. Accordingly, the value of 4.12 should be regarded as a nominal ductility index and interpreted together with the observed local damage, stiffness degradation, crack propagation, and poor panel-to-wall deformation compatibility, rather than as a fully developed ductility capacity.

The relatively low ductility coefficient of SW3 does not necessarily indicate typical brittle behavior. As observed in the test, SW3 did not experience a sudden loss of lateral resistance, and its cracking and damage developed progressively. The lower ductility coefficient was partly associated with the higher yield displacement and enhanced early-stage stiffness provided by the combined grouting and shear-key connection, which reduced the ratio between the ultimate displacement and the yield displacement. In addition, the test was terminated according to the predefined loading protocol when the specimen reached the specified damage or strength-degradation condition, which may have conservatively limited the further development of ultimate deformation. Therefore, the ductility coefficient of SW3 should be interpreted as the combined result of the strengthening mechanism and conservative test termination, rather than as direct evidence of brittle failure.

This displacement ductility coefficient alone is insufficient to evaluate the overall seismic performance of strengthened masonry walls. Although SW2 showed the highest ductility coefficient, its failure process was accompanied by severe diagonal cracking, large shear deformation of the masonry wall, and local crushing in the wall pier between openings. Therefore, the relatively large ductility of SW2 was associated with significant local damage and poor deformation compatibility between the precast concrete panel and the masonry wall. In comparison, SW3 exhibited a lower ductility coefficient but showed better crack control and more coordinated interaction between the two components. Overall, the seismic performance of different strengthening schemes should be evaluated comprehensively by considering ductility, bearing capacity, stiffness degradation, crack development, and panel-to-wall collaborative behavior.

4.3 Bearing capacity and lateral stiffness

In this study, the lateral stiffness K refers to the initial lateral stiffness of the specimen and was determined from the initial approximately linear segment of the skeleton curve before obvious cracking and stiffness degradation occurred. When both positive and negative loading branches were available, K was calculated as the average of the absolute stiffness values in the two loading directions:

$$K = \frac{1}{2}\left(\frac{|F_i^+|}{|\Delta_+|} + \frac{|F_i^-|}{|\Delta_-|}\right) \tag{2}$$

where F_i^+ and F_i^- are the lateral loads selected within the initial approximately linear ranges of the positive and negative loading branches, respectively, and Δ_i^+ and Δ_i^- are the corresponding lateral displacements. When only one loading direction was available, the slope of the initial approximately linear segment in that direction was used. Therefore, the lateral stiffness reported in Table 4 represents the initial lateral stiffness rather than the yield secant stiffness. The ultimate bearing capacity, initial yield force, and lateral stiffness of the four specimens are summarized in Table 4.

Table 4 Ultimate bearing capacity, yield force, and lateral stiffness of specimens

Specimen	SW1	SW2	SW3	SW4
Ultimate bearing capacity, F_u (kN)	450	433	415	76
Improvement ratio	5.92	5.70	5.46	1
Initial yield force, F_y (kN)	343	293	350	57.1
Improvement ratio	6.01	5.13	6.13	1
Lateral stiffness, K (kN/mm)	99.8	70.2	83	36.1
Improvement ratio	2.76	1.94	2.30	1

As shown in Table 4, SW4 was used as the unstrengthened control specimen for calculating the improvement ratios of bearing capacity, yield force, and lateral stiffness. Compared with the unstrengthened specimen SW4, the ultimate bearing capacities of specimens SW1, SW2, and SW3 increased by 5.92, 5.70, and 5.46 times, respectively. This indicates that all three strengthening schemes using externally attached precast concrete panels significantly improved the lateral load-bearing capacity of the masonry walls. Among the strengthened specimens, SW1 showed the highest ultimate bearing capacity of 450 kN, followed by SW2 and SW3, with ultimate bearing capacities of 433 kN and 415 kN, respectively. This result suggests that the grouting connection was particularly effective in mobilizing the precast concrete panel to participate in lateral load resistance through continuous interfacial bonding. Although the combined grouting and shear-key connection in SW3 was expected to provide both bonding and mechanical anchorage, the introduction of shear keys may have interrupted the continuity of the grouting interface and reduced the effective bonded area between the precast panel and the masonry wall. The local anchorage zones around the shear keys could also cause stress concentration and early microcracking in the surrounding masonry and grouting material. Therefore, SW3 did not exceed SW1 in terms of ultimate bearing capacity and initial lateral stiffness. Instead, its advantage was mainly reflected in improved deformation compatibility, crack control, and more balanced damage development.

It should also be noted that the post-cast concrete strength of SW1 was lower than that of SW2 and SW3. Nevertheless, SW1 still achieved the highest ultimate bearing capacity and lateral stiffness. This observation further suggests that the superior performance of SW1 was mainly associated with the effectiveness of the continuous grouting connection rather than with the strength of the post-cast concrete itself.

When the ultimate bearing capacity was reached, the corresponding displacements of specimens SW1, SW2, and SW3 were 20.5 mm, 37.9 mm, and 12.2 mm, respectively. Specimen SW2 reached the largest displacement among the three strengthened specimens, which is consistent with its relatively high displacement ductility coefficient. However, the larger deformation of SW2 was accompanied by severe diagonal cracking and local crushing in the wall pier between openings, as discussed in Section 3. Although the skeleton curve indicated that the bearing capacity of SW2 was still increasing before the termination of the test, the specimen had already suffered significant local damage. Therefore, the relatively large displacement reached by SW2 should be interpreted together with its damage state rather than as evidence of superior deformation capacity. As discussed in Section 4.2, its reported displacement ductility index represents a nominal index based on the available test response because the test was terminated before a complete post-peak response was obtained.

In terms of yield strength, SW3 exhibited the highest initial yield force of 350 kN, slightly higher than that of SW1 and significantly higher than that of SW2. The initial yield forces of SW1, SW2, and SW3 were 343 kN, 293 kN, and 350 kN, respectively, corresponding to improvement ratios of 6.01, 5.13, and 6.13 relative to SW4. This indicates that the combined grouting and shear-key connection enhanced the initial integrity of the strengthened wall system and delayed the onset of significant nonlinear deformation. The grouting layer provided continuous interfacial restraint, while the shear keys improved local mechanical anchorage. Their combined effect may have contributed to a higher yield resistance.

The lateral stiffness of the strengthened specimens was also significantly improved. Compared with SW4, the lateral stiffness values of SW1, SW2, and SW3 increased by 2.76, 1.94, and 2.30 times, respectively. SW1 had the highest lateral stiffness of 99.8 kN/mm, indicating that the grouting connection was most effective in improving the initial stiffness of the wall system. This is mainly because the continuous grouting layer enhanced the overall interaction between the precast concrete panel and the masonry wall. By contrast, SW2 showed the lowest stiffness improvement among the strengthened specimens, which can be attributed to the discrete nature of the shear-key connection. Since the shear force was transferred mainly through localized mechanical interlocking, the overall interfacial restraint was weaker than that provided by a continuous grouting layer.

Overall, the results in Table 4 demonstrate that externally attached precast concrete panels can substantially enhance the bearing capacity and lateral stiffness of masonry walls. The grouting connection was more effective in improving ultimate bearing capacity and initial stiffness, while the combined grouting and shear-key connection provided the highest yield force among the strengthened specimens. Although the shear-key connection improved deformation capacity, it was less effective in controlling local damage and stiffness degradation. Therefore, the strengthening performance should be evaluated comprehensively by considering ultimate bearing capacity, yield force, lateral stiffness, deformation capacity, and damage development.

5. Discussion on the Strengthening Mechanism

The experimental results indicate that the seismic improvement of masonry walls strengthened with externally attached precast concrete panels is strongly influenced not only by the additional stiffness and strength provided by the panels, but also by the load-transfer mechanism at the interface between the precast panels and the original masonry walls. Under cyclic lateral loading, the original masonry wall mainly resisted horizontal action through the wall pier between openings. As damage progressed, diagonal cracks initiated at the window corners and gradually propagated into the wall pier, leading to shear deformation, stiffness degradation, and local crushing. After strengthening, the externally attached precast concrete panel participated in lateral load resistance and helped restrain deformation of the masonry wall, thereby improving the overall seismic performance of the wall system.

For specimen SW1, the grouting connection provided a relatively continuous interfacial bonding layer between the precast concrete panel and the masonry wall. This continuous connection enabled the panel and the masonry wall to work together during early loading, resulting in higher initial lateral stiffness and ultimate bearing capacity. As shown in Table 4, SW1 exhibited the highest ultimate bearing capacity and lateral stiffness among the strengthened specimens. This indicates that the grouting layer was effective in mobilizing the precast concrete panel to resist lateral loads. From a mechanical perspective, the grouting layer distributed interfacial shear, reducing reliance on localized force-transfer points. Therefore, the grouting connection was more favorable for improving the global load-bearing capacity and stiffness of the strengthened wall. However, under large cyclic deformation, repeated crack opening and closing may have reduced the interfacial restraint to some extent, as reflected by the observed deformation incompatibility between the panel and the masonry wall.

For specimen SW2, the shear-key connection mainly relied on localized mechanical interlocking to transfer shear force between the precast panel and the masonry wall. This connection allowed the specimen to develop a relatively large displacement after yielding, and SW2 exhibited the highest displacement ductility coefficient among the strengthened specimens. However, the test phenomena showed that this deformation capacity was accompanied by severe diagonal cracking and local crushing in the wall pier between openings. Table 2 further demonstrates that the deformation compatibility between the precast panel and the masonry wall was poor in SW2. At a displacement amplitude of +25 mm, the diagonal displacement of the precast panel was only 5.5 mm, whereas that of the masonry wall reached 49.8 mm. This large difference indicates that the shear deformation was mainly concentrated in the masonry wall rather than being effectively shared by the precast panel. Therefore, although the shear-key connection enhanced local anti-slip resistance, it also led to localized stress concentrations in the shear-key regions, which were associated with accelerated crack development and damage accumulation.

For specimen SW3, the combined grouting and shear-key connection integrated continuous interfacial bonding with localized mechanical anchorage. The grouting layer improved the overall contact and deformation coordination between the precast panel and the masonry wall, while the shear keys provided additional anti-slip resistance and local anchorage. This combined mechanism allowed the horizontal load to be transferred through both distributed interfacial bonding and localized mechanical interlocking. However, the addition of shear keys did not simply produce a linear superposition of the advantages of grouting and mechanical anchorage. From a physical perspective, the shear-key regions changed the originally continuous grouting interface into a locally discontinuous interface, which may have weakened the uniformity of interfacial stress transfer. At the same time, the geometric discontinuity and stiffness mismatch around the shear keys could induce local stress concentration, microcrack initiation, and local crushing of the adjacent masonry or grouting material. These effects reduced the contribution of continuous interface bonding to the initial lateral stiffness and ultimate bearing capacity. As a result, SW3 exhibited more stable damage development and better crack control than SW2. The diagonal displacement difference between the precast panel and the masonry wall was also smaller in SW3, indicating better collaborative deformation. Although SW3 did not show the highest ultimate bearing capacity or displacement ductility, it exhibited the highest initial yield force and a more balanced seismic response. Therefore, the advantage of SW3 should be understood as comprehensive seismic performance rather than maximum peak strength or maximum initial stiffness.

The different strengthening mechanisms can also explain the hysteretic and energy dissipation behavior of the specimens. The relatively full hysteretic loops of SW1 and SW3 indicate that both grouting-based schemes provided better integrity and more stable load-transfer capacity during cyclic loading. In contrast, SW2 showed significant stiffness degradation and severe pinching, associated with diagonal crack opening and closing, local sliding, and damage concentration in the masonry wall. Although SW2 exhibited relatively high cumulative energy dissipation at large displacement amplitudes, this dissipation was mainly due to severe cracking and local crushing. Therefore, high energy dissipation alone does not necessarily represent favorable seismic performance when it is accompanied by excessive local damage and loss of vertical load-bearing capacity.

Based on the above analysis, the strengthening mechanism of externally attached precast concrete panels can be summarized as follows. First, the precast panel provides an additional lateral resisting component, improving the overall stiffness and load-bearing capacity of the masonry wall. Second, the connection system determines whether the panel can effectively participate in load resistance. A continuous grouting connection improves bearing capacity and initial stiffness, while a shear-key connection enhances local mechanical interaction and deformation capacity. Third, the combined grouting and shear-key connection provides a more balanced load-transfer path, reduces excessive deformation incompatibility, and improves crack-control performance. Therefore, from the perspective of strengthening mechanisms, the seismic performance of externally strengthened masonry walls should be evaluated not only by strength and ductility, but also by interfacial load transfer, deformation compatibility, local damage development, and the potential residual safety of the masonry wall.

For practical application, the connection design should avoid excessive concentration of shear force at limited anchorage regions. When shear keys are used, their spacing and anchorage depth, together with the quality of the surrounding grouting material, should be carefully controlled to reduce local stress concentration and the risk of masonry crushing. When a grouting connection is adopted, the bonding quality and durability of the interface should be ensured to maintain composite action under repeated loading. The combined grouting and shear-key connection may be considered when both structural safety and deformation compatibility are required, as it leverages the advantages of continuous bonding and mechanical anchorage.

6. Conclusions

This study experimentally investigated the seismic performance of masonry walls strengthened with externally attached precast concrete panels using three different panel-to-wall connection configurations: grouting, shear keys, and a combined grouting–shear-key connection. The strengthening effectiveness was evaluated through the observed failure modes, hysteretic behavior, bearing capacity, lateral stiffness, deformation capacity, and deformation compatibility between the precast panels and masonry walls. Based on these experimental and comparative results, the following conclusions can be drawn:

(1) The effectiveness of the externally attached precast concrete panels depended primarily on the reliability of the panel-to-wall load-transfer mechanism. When effective interaction was established, the precast panel participated in resisting lateral loads, restrained crack propagation, and improved the overall integrity of the masonry wall system.

(2) The grouting connection provided the most significant improvement in bearing capacity and initial stiffness. The continuous grouting layer enabled distributed interfacial shear transfer and promoted composite action between the precast panel and the masonry wall. Therefore, this connection is more suitable when enhancing lateral resistance and initial stiffness is the primary strengthening objective.

(3) The shear-key connection improved the nominal deformation capacity but caused severe local damage. Although SW2 exhibited the highest nominal ductility coefficient, its response was accompanied by pronounced diagonal cracking, local crushing, and poor deformation compatibility. This indicates that the relatively large deformation of SW2 was achieved at the cost of concentrated damage in the masonry wall. Therefore, the shear-key connection should be used cautiously as the sole connection mechanism when crack control and residual safety are important.

(4) The combined grouting and shear-key connection showed the most balanced seismic performance. Although SW3 did not achieve the highest peak strength or ductility coefficient, it exhibited better crack control, higher yield resistance, and improved deformation compatibility between the precast panel and the masonry wall. These results indicate that the combined connection may be advantageous when balanced performance, damage control, and deformation compatibility are prioritized over maximum bearing capacity alone.

(5) The proposed prefabricated strengthening method has potential for low-disturbance seismic rehabilitation of existing masonry walls. However, because only one specimen was tested for each configuration, the results should be regarded as preliminary comparative trends. In addition, the specimens did not experience completely identical force-controlled loading histories, and the test of SW2 was terminated prematurely because of severe local damage. Future studies should include repeated specimens, adopt more consistent loading histories, and further examine the effects of panel thickness, shear-key spacing, grouting quality, axial compression ratio, and opening configuration.

Conflicts of Interest

The authors declare no conflict of interest.

References

[1] I. Hafner, T. Kišiček, and M. Gams, "Review of Methods for Seismic Strengthening of Masonry Piers and Walls," Buildings, vol. 13, no. 6, article no. 1524, 2023.

[2] A. Keshmiry, S. Hassani, U. Dackermann, and J. Li, "Assessment, Repair, and Retrofitting of Masonry Structures: A Comprehensive Review," Construction and Building Materials, vol. 442, article no. 137380, 2024.

[3] A. Majumder, F. Stochino, M. Valdes, G. Concu, M. Pepe, and E. Martinelli, "Sustainable Masonry Retrofitting and Upgrading Techniques: A Review," Fibers, vol. 13, no. 6, article no. 68, 2025.

[4] S. Petrovčič, P. Prašnikar, and V. Kilar, "Seismic Assessment and FRCM Strengthening of Post-War Masonry Residential Buildings: A Case Study on Building Typologies," International Journal of Disaster Risk Reduction, vol. 119, article no. 105341, 2025.

[5] N. Gattesco, E. Rizzi, I. Boem, A. Dudine, and M. Gams, "Seismic Strengthening of Existing Brick Masonry with CRM Coatings on One Side," Bulletin of Earthquake Engineering, vol. 23, no. 9, pp. 3779-3808, 2025.

[6] N. Gattesco, E. Rizzi, I. Boem, A. Dudine, and M. Gams, "A New Method of Seismic Strengthening Stone Masonry with CRM Coatings on One Side," Construction and Building Materials, vol. 407, article no. 133565, 2023.

[7] M. Scamardo, S. Cattaneo, P. Crespi, and L. Biolzi, "Design Method for Masonry Structures Retrofitted with Steel Reinforced Plaster," Journal of Building Engineering, vol. 79, article no. 107828, 2023.

[8] M. Scamardo, S. Cattaneo, and P. Crespi, "Masonry Retrofitting with Steel Reinforced Plaster: Experimental and Analytical Study," Journal of Building Engineering, vol. 108, article no. 112890, 2025.

[9] L. Pérez-Pinedo, C. Sandoval, R. Alvarado, L. Vargas, S. Calderón, and E. Bernat, "Seismic Strengthening of Partially Grouted Masonry Walls with Openings: Evaluation of Ferrocement and BTRM Solutions," Journal of Building Engineering, vol. 88, article no. 109235, 2024.

[10] P. Tian, W. Yang, C. Cao, Z. Bian, Z. Yun, and J. Lu, "A Study of the Seismic Resistance Performance of Strengthened Masonry Walls Using Polypropylene Mesh-Composite on the Surface," Structures, vol. 68, article no. 107270, 2024.

[11] S. Jafarian, M. Esmaelian, M. Shekarchi, and M. Ghassemieh, "Performance of Low-Carbon Textile-Reinforced Mortar: Out-of-Plane Response of Strengthened Masonry Walls," Construction and Building Materials, vol. 415, article no. 134904, 2024.

[12] N. Tarifa, Z. I. Djamai, and F. Duprat, "Effect of Textile Reinforced Mortar Components on the Mechanical Behavior of Historical Masonry Structures under Cyclic Loading," Journal of Building Engineering, vol. 83, article no. 108334, 2024.

[13] F. Qu, S. Yin, F. Wang, and B. Wang, "Effects of Textile-Reinforced Concrete on the Cyclic Shear Behavior of Damaged Confined Brick Masonry Walls," Journal of Building Engineering, vol. 78, article no. 107717, 2023.

[14] S. Shahzamani and M. R. Eftekhar, "Experimental Study on Using Steel Wires via the NSM Method to Improve the Behaviour of Masonry Panels," Construction and Building Materials, vol. 385, article no. 131473, 2023.

[15] M. Scamardo, S. Cattaneo, P. Crespi, and N. Vafa, "Cyclic Behavior of C-Shaped Masonry Wall Retrofitted with Twisted Bars or Bonded Rebars," Construction and Building Materials, vol. 443, article no. 137703, 2024.

[16] X. Sun, P. Shi, H. Zhu, Z. Dong, B. Mu, and C. K. Soh, "Shear Performance of Brick Masonry Walls Strengthened by Deep Structural Repointing Using FRP Reinforcement," Journal of Building Engineering, vol. 111, article no. 113187, 2025.

[17] X. Sun, H. Zhu, P. Shi, Z. Dong, G. Zhang, and Y. Pan, "Strengthening Masonry Walls by Self-Prestressing Reinforced Repointing Using Fe-SMA Materials: A Feasibility Study," Construction and Building Materials, vol. 502, article no. 144340, 2025.

[18] A. Alaskar, M. Ghalla, R. W. Bazuhair, G. Elsamak, M. Emara, and M. A. Altobgy, "Seismic Rehabilitation of Brick Masonry Walls with Central Openings Using Hybrid GFRP Configurations," Journal of Building Engineering, vol. 111, article no. 113464, 2025.

[19] E. A. Mlybari, M. Ghalla, J. W. Hu, R. W. Bazuhair, M. A. Altobgy, and A. A. Alkhawaldeh, "Value-Oriented SHCC-Based Strengthening of Masonry Walls with Openings: Integration of Glass Fiber Mesh and Steel Bars for Seismic Risk Mitigation in Construction," Case Studies in Construction Materials, vol. 23, article no. e05511, 2025.

[20] L. Pérez-Pinedo, C. Sandoval, L. Vargas, and R. Alvarado, "In-Plane Cyclic Response of Partially Grouted Masonry Walls Repaired and Retrofitted with SRG Strips," Engineering Failure Analysis, vol. 182, part B, article no. 110078, 2025.

[21] C. Mollamahmutoglu, M. Ozturk, and M. O. Yilmaz, “Shear Capacity of Masonry Walls Externally Strengthened via Reinforced Khorasan Jacketing,” Buildings, vol. 15, no. 13, article no. 2177, 2025.

[22] Z. U. Abidin, K. Shahzada, A. Gul, Y. Alqaryouti, M. Azab, M. Rizwan, et al., “Strengthening of Masonry Infill Wall Panels in Reinforced Concrete Structures Using Dual Strengthening Strategy of Ferrocement and ECC Overlays,” Cogent Engineering, vol. 11, no. 1, article no. 2388794, 2024.

[23] W. Tan, T. Zhou, L. Zhu, X. Zhao, W. Yu, L. Zhang, et al., “Seismic Performance of a Single-Story Timber-Framed Masonry Structure Strengthened with Fiber-Reinforced Cement Mortar,” Materials, vol. 17, no. 15, article no. 3644, 2024.

[24] P. Foraboschi, “Shear Strength of a Dowel Plate Anchored to a Masonry Wall,” Engineering Structures, vol. 329, article 119773, 2025.

[25] Y. Q. Zhang, X. C. Lin, T. Wang, and K. Skalomenos, “Seismic Behavior of Masonry Walls Strengthened by Precast Reinforced Concrete Panels with Different Connection Details,” Engineering Structures, vol. 242, article no. 112597, 2021.